https://doi.org/10.1016/j.energy.2023.128402

Three-dimensional yaw wake model development with validations from wind tunnel experiments

Ruiyang He[a] *, Xiaowei Deng[b], Yichun Li[a], Zhikun Dong[b], Xiaoxia Gao[c], Lin Lu[a], Yue Zhou[d], Jianzhong Wu[d], Hongxing Yang[a] *

a Renewable Energy Research Group (RERG), Department of Building Environment and Energy Engineering, The Hong Kong Polytechnic University, Hong Kong

b Department of Civil Engineering, The University of Hong Kong, Pokfulam, Hong Kong

c Department of Power Engineering, North China Electric Power University (Baoding), China

d Cardiff University, Cardiff CF24 3AA, UK

* Corresponding author

E-mail address: ruiyang.he@connect.polyu.hk; hong-xing.yang@polyu.edu.hk

Abstract

The presence of wake flows caused by wind turbines (WTs) diminish the expected power generation of wind energy and exacerbate structural vibrations. To mitigate these issues, yaw control has emerged as a promising technique for intentionally deflecting the wake away from downstream WTs. Consequently, accurate prediction of the yawed wake is of paramount importance for effective implementation of yaw control strategies. This study presents an innovative and comprehensive approach to modeling yaw wake behavior by introducing an advanced three-dimensional yaw wake model. This model incorporates anisotropic and general expressions of the wake expansion rate, allowing for a more accurate and physically meaningful representation of wake evolution. More importantly, the easily-available parameters in the function guarantee the generalization capability of the proposed model. Subsequently, a wake deflection mode is developed and integrated into the yaw wake model through the inclusion of a deflection term. To validate the proposed models, two sources of data are utilized. Firstly, well-known public measurements are used to verify the accuracy and reliability of the model predictions. Secondly, wind tunnel experiments are conducted by the authors, employing a particle image velocimetry (PIV) system to capture detailed flow field information. This combination of validation sources ensures a comprehensive assessment of the proposed models. The physical description and error analysis conducted in this study

reveals that the proposed model outperforms other models in terms of predicting wake distribution and the trajectory of the deflected wake centreline. In particular, the comparative analysis confirms its superior performance in the main angle and downstream region that are of particular interest for active yaw control. The accurate and cost-efficient nature of the proposed analytical yaw wake model holds great potential for optimizing yaw control strategies in wind farms. This study is expected to contribute to the field by offering a reliable and practical tool for understanding and managing the effects of yaw operation on wake behavior.

Keywords: *Wind tunnel experiment; wind turbine; PIV measurements; yaw wake model*

Nomenclature

List of abbreviations

3-D	three-dimensional
ABL	atmospheric boundary layer
ADM	actuator disk model
ALM	actuator line model
CFD	computational fluid dynamics
CVP	counter-rotating vortex pair
D	the rotor diameter of the wind turbine
FOV	field of view
LES	large eddy simulation
RANS	Reynolds-averaged Navier-Stokes
PIV	particle image velocimetry
WT	wind turbine

List of symbols

$A(x)$	parameter in yaw wake model(m^3/s)
A_0	swept area of the rotor (m^2)
a	axial induction factor
C_T	thrust force coefficient
h_0	hub height of wind turbine (m)
I_0	turbulence intensity
r_0	wind turbine rotor radius (m)
r_1	initial wake radius (m)
r_y	wake radius in horizontal (Y) direction (m)
r_z	wake radius in vertical (Z) direction (m)
T	thrust force (N)
u_0	inflow wind speed (m/s)
$U(x,y,z)$	wake velocity under uniform inflow (m/s)
$U_w(x,y,z)$	wake velocity under shear inflow (m/s)
k_{Jensen}	wake expansion rate in the Jensen model
k_y	horizontal wake expansion rate
k_z	vertical wake expansion rate
$S_{elliptical}$	elliptical wake area at any downstream location (m2)
γ	yaw angle
θ	skew angle
$\sigma(x)_y$	horizontal standard deviation (m)
$\sigma(x)_z$	vertical standard deviation (m)
α	power-law exponent
ρ	air density (kg/m3)
δ_y	horizontal wake deflection (m)

1. Introduction

With the escalation of energy crisis and the impending deadline for carbon emission peak, the significance of renewable energy is becoming increasingly pronounced. In this context, wind energy has emerged as a highly promising and rapidly expanding source of renewable energy, poised to assume a vital role in global energy consumption. As reported by the global wind energy report [1], in order to achieve the wind energy capacity required by 2030 for a 1.5℃ and net zero pathway, 150 GW of new global installation is demanded this year (the year 2023). However, the presence of wake effects experienced by downstream wind turbines within a wind farm can have detrimental consequences, such as reduced power output and increased turbulence. These effects compromise the advantages of high capacity and cost-effectiveness, presenting substantial challenges to the efficient and economic operation of wind farms.

In order to alleviate the adverse impacts associated with wake flow, various strategies for wake control have been proposed [2]. Among them, yaw control is one of the most widely adopted and effective active wake control methods [3]. Recent research has demonstrated that intentionally deflecting the wake away from the downstream wind turbines holds significant potential for enhancing power generation across the entire wind farm [4,5]. Dou et at. [6] optimized the yaw angles of the well-known Horns Rev offshore wind farm and found that up to 7% power enhancement could be achieved depending on the wind directions and that the narrow spacing between wind turbines facilitated the optimized returns. Research from Ref. [7] complements that high turbulence and mean inflow speed can also bring better yaw optimization effectiveness, including both power gains and load mitigation. Moreover, Fleming et al. [8] conducted a series of field campaign of yaw wake control and indicated that for two closely installed wind turbines, 4% power enhancement of the two-wind turbine pair were measured. Zong [9] further concluded that the active yaw control is able to improve 7% to 13% of total power generation with aligned layouts while remarkably mitigating the power variability of the downstream wind turbines.

On the other hand, the phenomenon of wake deflection, which constitutes a crucial aspect of yawed wake development, has been the subject of extensive investigation regarding its evolution and distinctive characteristics. . By conducting wind tunnel tests with a hot wire anemometer, Medici et al. [10] found that the transverse velocity induced by yawed rotor was the reason for wake deflection. Furthermore, a deeper investigation was performed by Howland et al. [11] by using both wind tunnel measurements and large eddy simulation (LES) coupled with the actuator disk model (ADM) and actuator line model (ALM). Their results

demonstrated that rather than uniform distribution, the distribution of transverse velocity is more like a counter-rotating vortex pair (CVP) with its boundary approximately at the hub height, which can not only convect the wake flow laterally but also deform it into a curled shape. Furthermore, Bastankhah and Porté-Agel [12] explained the wake deflection from the point of view of continuity and Reynolds-averaged Navier-Stokes (RANS) equations. The kidney-shape deformation of wake cross-section due to wake steering was also found, but the researchers indicated that this phenomenon is not that noticeable if the yaw angle is less than 30° and therefore it can be simplified to elliptical wake distribution with a slower wake expansion rate in the horizontal direction.

Despite the comprehensive investigation of wake deflection and yawed wake distribution using wind tunnel experiments and computational fluid dynamic (CFD) methods, their direct application in yaw optimization strategies is hindered due to high computational cost or experimental expense. Given the dynamic nature of inflow conditions, which encompass variables such as wind speed, turbulence, and wind direction, there is a pressing need for a cost-efficient and accurate analytical yaw wake model. Such a mode is expected to play a crucial role in determining the optimal yaw angle for each wind turbine (WT) during the process of yaw optimization. Jimenez et al. [13] developed the first yaw wake model based on the 1D Jensen model [14] and therefore also gave a top-hat shape yawed wake prediction. A concept of control volume was adopted to conduct momentum conservation between the far upstream and yawed wake by neglecting the pressure term. Then the wake deflection was considered to be induced by the lateral component of thrust force. However, the Jimenez model has been proved to tend to overestimate the skew angle and transverse velocity magnitudes in the yawed wake [9,15]. Based on a framework similar to the Jimenez model [13], Qian and Ishihara [16] proposed a more advanced three-dimensional (3D) yaw wake model while also applying momentum conservation over a control volume. In contrast to the previous top-hat counterpart, the wake flow was considered Gaussian distribution with a self-similarity assumption. The expression with generalization capability for wake expansion was given by the proposed model while assuming the uniform expansion rates in vertical and horizontal directions under yaw operations. By performing wind tunnel tests and theoretical investigation on yawed wake, Bastankhah and Porté-Agel [12] developed a yaw wake model based on simplified RANS. The proposed yaw wake model is also based on 3D Gaussian distribution but had two different wake expansion rates in two directions to represent the elliptical cross-section in the far wake caused by wake deflection. Shapiro et al. [15] modeled

the rotor as an elliptically loaded lifting body. Like the other models, the streamwise wake distribution was obtained by using the momentum law. Interestingly, the Prandtl's lifting line method, instead of the classical momentum theory, was employed to correlate the transverse velocity and the lateral thrust force of a yawed WT. Unfortunately, the previous yaw wake models have relied on posterior wake expansion rates derived from experimental data, thus confining their applicability to specific environmental and operational conditions. Consequently, the existing yaw wake models either lack sufficient accuracy or oversimplify the consideration of anisotropic wake distribution induced by yaw operations., too simplified to account for the anisotropy of wake expansion rates due to yaw operations or use one or two posterior wake expansion rates that lack generalization capability.

To solve the remained challenges as discussed above, in this study, a 3D yaw wake model is proposed to accurately predict the wake deflection caused by yaw operations and yawed wake distribution. Compared with the existing models, the main contributions of the yaw wake model are listed as follows. 1) The advanced 3D wake model previously developed by the author is used to derive the yaw wake model, which ensures its accuracy without considering the wake deflection term. 2) The proposed model adopts anisotropic wake expansion rates in the horizontal and vertical direction instead of uniform ones, not only because of the ground effects or incoming boundary-layer condition found in unyawed conditions but, more importantly, because of the elliptical cross-section of wake distribution caused by yaw operation. 3) The given anisotropic expression of the wake expansion rates is a function of the thrust coefficient, the turbulent intensity at hub height, and the yaw angle, which guarantees their ability to generalize to different environmental and operational conditions while ensuring the ease of use of the proposed yaw wake model.

The whole paper is structured in the following way. In Section 2, the derivation process of the novel 3D anisotropic yaw wake model is given, followed by the validation from wind tunnel experiments obtained from public literature in Section 3. Then, in Section 4, the wind tunnel measurements are conducted and the results are employed for model verification. Finally, the last section gives a summary and conclusions.

2. Yaw wake model development

An analytical yaw wake model will be derived based on the previously developed three-dimensional elliptical Gaussian shape wake model (3DEG model) [17] for normal wake

prediction to integrate the effects of yaw misalignment on wake development. The proposed model will be accurate, computationally efficient, and easy to use with explicit expression.

To demonstrate the wake evolution and deflection clearly, as shown in Fig. 1, a 3D coordinate system is established first with the origin at the bottom of the wind turbine tower, of which the positive X-axis refers to the inflow direction, Y-axis is the radial direction, and the direction in which the wake steering takes place, and the positive Z-axis denotes the direction of vertical ground upward.

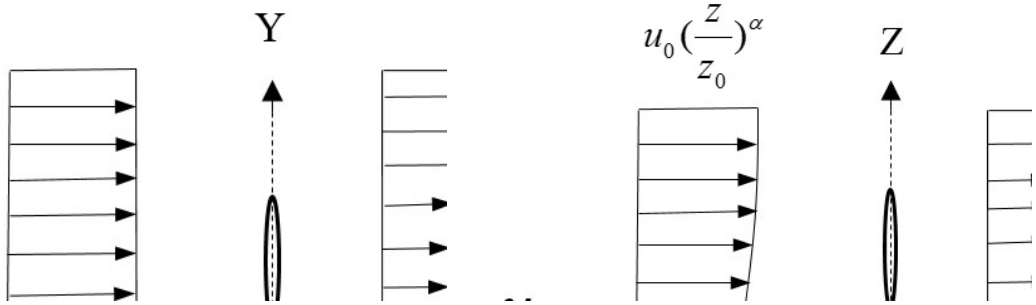

(a) Horizontal plane (b) Vertical plane

Fig.1 Schematic diagram of wake expansion in the vertical and horizontal direction [17].

2.1 Model derivation under uniform inflow

To ensure simplicity during the development of the yaw wake model, an initial assumption of uniform inflow is made. The yaw wake model bears resemblance to the wake model during regular operations, yet it introduces an additional deflection term δ_y. This term accounts for the horizontal displacement of the wake centreline due to yaw operation and is dependent on the yaw angle and distance downstream.

As stated in the previous study [18,19], the wake growth rate of a non-yawed wind turbine might be different in the vertical and horizontal direction due to the ground effects or vertically sheared turbulence. More significantly, the wake cross-section of a yawed wind turbine should exhibit an elliptical shape, featuring a wider dimension in the vertical direction and a narrower dimension in the horizontal direction, due to the wake deflection. Consequently, as given in Eq. (1), an anisotropic 2D Gaussian function with elliptical cross-section is proposed here to account for the phenomena explained before. Note that the Gaussian function is defined by its mean (μ) and standard deviation (σ), which determine its center and spread, respectively. By employing two different mean values (δ_y and h_0) and

two standard deviations (σ_y and σ_z) in Eq. (1), it means that an elliptical Gaussian function is adopted.

$$U(x,y,z) = u_0 - \frac{A(x)}{2\pi\sigma(x)_y\sigma(x)_z} e^{-\left(\frac{(y-\delta_y)^2}{2\sigma(x)_y^2}+\frac{(z-h_0)^2}{2\sigma(x)_z^2}\right)} \quad (1)$$

where A(x) is an unknown parameter that needs to be determined and depends on the downwind distance.

To determine the wake boundary layer, a 99% wake recovery compared to the surrounding free flows is usually adopted [17]. As the 2D Gaussian function is adopted in this model, the elliptical-shape confidence region representing the 99% probability denotes the probability that each dimension should satisfy the 99% square root. Accordingly, the relationship between standard deviation and wake radius is built as shown in Eq. (2). Note that due to the wake deflection, the standard deviation in the horizontal direction $\sigma(x)_y$ and therefore the wake radius is different from those of a non-yawed wind turbine, even though they have the same expression.

$$r_y = 2.81\sigma(x)_y,\ r_z = 2.81\sigma(x)_z \quad (2)$$

As the wake evolution follows the mass and momentum law [20], Eq. (3) is given by neglecting the pressure terms and viscous in the momentum equation.

$$\rho\int U(x,y,z)[u_0 - U(x,y,z)]dA = T \quad (3)$$

where T is the thrust force under yaw conditions and can be expressed as [21]:

$$T = \frac{1}{2} C_T \rho A_0 {u_0}^2 \cos^2\gamma \quad (4)$$

where the thrust coefficient Ct, rotor swept area A_0, and inflow wind speed u_0 denote their corresponding values under non-yawed conditions. The loss of thrust force caused by yaw operations makes it smaller than the original value by $\cos^2\gamma$.

By combining Eq. (1), (3), and (4), the following equation can be derived:

$$\frac{1}{4\pi\sigma(x)_y\sigma(x)_z} A^2 - u_0 A + \frac{1}{2} C_T A_0 {u_0}^2 \cos^2\gamma = 0 \quad (5)$$

And one of the two solutions that satisfies the physical meaning is shown below:

$$A = 2\pi\sigma(x)_y\sigma(x)_z u_0(1-\sqrt{1-\frac{C_T r_0^2\cos^2\gamma}{2\sigma(x)_y\sigma(x)_z}}) \tag{6}$$

Therefore, the yaw wake model under uniform inflow can be obtained:

$$U(x,y,z) = u_0(1-(1-\sqrt{1-\frac{C_T r_0^2\cos^2\gamma}{2\sigma(x)_y\sigma(x)_z}})e^{-(\frac{(y-\delta_y)^2}{2\sigma(x)_y^2}+\frac{(z-h_0)^2}{2\sigma(x)_z^2})}) \tag{7}$$

As concluded by Bastankhah and Porté-Agel [22], the wake expansion rate in the horizontal direction would not be affected by yaw operations. However, the initial value of standard deviation, ε_Y in the proposed yaw wake model, would be $\cos\gamma$ smaller than that under normal conditions. Therefore, based on our previously developed 3DEG model [17], the expression of two standard deviations can be expressed as follows:

$$\frac{\sigma_y}{D} = k_y\frac{x}{D} + \varepsilon_y\cos\gamma\,,\ \frac{\sigma_z}{D} = k_z\frac{x}{D} + \varepsilon_z \tag{8}$$

$$k_Y = 0.065C_T^{\,0.2566}I_0^{\,0.2808}\,,\ k_Z = 0.0866C_T^{\,0.4279}I_0^{\,0.4707} \tag{9}$$

$$\varepsilon_Y = 0.2406C_T^{0.1147}I_0^{0.0124}\,,\ \varepsilon_Z = 0.2788C_T^{0.0295}I_0^{0.032} \tag{10}$$

2.2 Wake deflection model

The next step is to determine the wake deflection term δ_y in the proposed yaw wake model. As shown in Eq. (13), finding the wake deflection δ_y can be first reduced to finding the skew angle θ. Consequently, the concept of control volume proposed by Jimenez [13], is used here to establish the relationship between the far upstream and the deflected wake, so that the skew angle can be defined according to the law of momentum conservation. Under this assumption, the thrust force of the yawed wind turbine is equal to the momentum of the control body outlet minus the momentum of the inlet and that caused by flow entrainment. However, since neither of the latter two has a component in the radial direction, the thrust force projected to the radial direction is balanced by the spanwise component of the momentum at the control body outlet. The expression can be given as:

$$T\sin\gamma = \rho\iint U^2(x,y,z)\sin\theta(x)\,dA \tag{11}$$

The skew angle is the angle between the original wake center line and the deflected one, whose initial value is much smaller than the corresponding yaw angle and continues to decrease as the distance downstream increases. Therefore, it is safe to take an approximation of $\sin\theta(x)\approx\theta(x)$ in far wake region under yaw control. By inserting Eq. (7) into Eq. (11), the expression of the skew angle can be obtained:

$$\theta(x)=\frac{T\sin\gamma}{\rho\iint U^2(x,y,z)dA}=\frac{\frac{1}{2}C_T r_0^{\,2}\cos\gamma\sin\gamma}{7.9\sigma(x)_y\sigma(x)_z-C_T r_0^{\,2}\cos\gamma} \tag{12}$$

According to its physical meaning, the skew angle can also be written as the derivative of wake deflection δ_y:

$$\theta(x)=\frac{d\delta_y(x)}{dx} \tag{13}$$

In order to determine the deflection term added in the yaw wake model, a common practice is to set an initial condition of the far wake region [12,15,16]. Then the wake deflection in the far wake region can be obtained by integrating the skew angle from the onset condition and replacing the dx by $\frac{1}{k}d(\sigma/D)$ according to Eq. (8):

$$\frac{\delta_y(x)}{D}=\frac{1}{D}\int_{x_0}^{x}\theta(x)dx+\frac{\delta_{y0}}{D}=\frac{1}{k}\int_{\sigma_0/D}^{\sigma/D}\theta(\sigma/D)d(\sigma/D)+\frac{\delta_{y0}}{D} \tag{14}$$

where the wake expansion rate and the standard deviation shown in the equation above can be determined by taking the square root of the values in horizontal and vertical directions [12]:

$$k=\sqrt{k_y k_z}\ ,\ \sigma=\sqrt{\sigma_y\sigma_z} \tag{15}$$

Then, the expression of wake deflection in the far wake region can be given as:

$$\frac{\delta_y(x)}{D}=\frac{r_0\sin\gamma\sqrt{C_T\cos\gamma}}{11.24k}\ln\left|\frac{\left(\sigma_0/D+0.356r_0\sqrt{C_T\cos\gamma}\right)\left(\sigma/D-0.356r_0\sqrt{C_T\cos\gamma}\right)}{\left(\sigma_0/D-0.356r_0\sqrt{C_T\cos\gamma}\right)\left(\sigma/D+0.356r_0\sqrt{C_T\cos\gamma}\right)}\right|+\frac{\delta_{y0}}{D} \tag{16}$$

The above equation is applicable only in the far wake region under yaw control since it is developed based on the control volume concept and the momentum conservation law employed on it. Therefore, going for the initial skew angle, initial wake deflection, and the joint location that initial wake deflection equals to that in the far wake region is still required.

In analogy to the skew angle of a helicopter rotor proposed by Coleman [23], the initial value of the skew angle of yawed wind turbine rotor θ_0 is also considered to be constant and expressed as follows:

$$\theta_0 = \frac{0.3\gamma}{\cos\gamma}\left(1-\sqrt{1-C_T\cos\gamma}\right) \tag{17}$$

As concluded by a previous study [12], the wake deflection in the near wake region increases almost linearly as a function of the initial skew angle and the corresponding downstream location when $x \leq x_0$ and can be written as below:

$$\frac{\delta_y(x)}{D} = \theta_0 \frac{x}{D} \tag{18}$$

Since the predicted skew angle should be continuous from the near wake to the far wake region, their value should be the same at the joint location. By equating Eq. (17) and Eq. (12) with their value at the joint location x_0, the standard deviation at the far wake onset place can then be found:

$$\frac{\sigma_0}{D} = \sqrt{\frac{C_T r_0^2 \cos\gamma\left(\sin\gamma + 2\theta_0\right)}{15.8\theta_0}} \tag{19}$$

Please note that due to wake deflection, the standard deviation in two directions has different formats, of which the initial value ε_Y in the horizontal direction is $\cos\gamma$ smaller as demonstrated in Eq. (8). Therefore, the standard deviation at the joint location can also be given as:

$$\frac{\sigma_0}{D} = \sqrt{\left(k_y\frac{x_0}{D} + \varepsilon_y\cos\gamma\right)\left(k_z\frac{x_0}{D} + \varepsilon_z\right)} \tag{20}$$

Finally, the value of x_0 can be calculated by equating Eq. (19) and (20) and adopting the one with practical meaning. As indicated by Bastankhah and Porté-Agel [22], the above estimation of x_0 does not aim to accurately predict the near wake length but gives an initial value for the yawed wake prediction in the far wake model, which would be the main interest of active yaw control.

2.3 Model extension with shear inflow

As the former derivation process neglects the wind speed variation in the vertical direction, the model derived in Sections 2.1 and 2.2 needs to be further developed to consider shear inflow and its effects on wake deflection. The wind power law is employed in this study to represent the shear inflow conditions. The inflow difference between shear inflow and uniform inflow can be given as:

$$\Delta u = u_0(\frac{z}{z_0})^{\alpha} - u_0 \tag{21}$$

Therefore, the mass difference in the wake region resulting from the inflow difference can be decomposed into two parts: the mass obtained by integrating the initial speed difference $\Delta u(1-2a)$ over the area swept by the initial wake radius r_1 and the mass obtained by integrating the wind speed difference over the rest of wake region [24].

$$\Delta m = \iint_{Sr_1} \Delta u(1-2a)dA + \iint_{S_{elliptical}-Sr_1} \Delta u dA \tag{22}$$

In which, the initial wake radius denotes the wake radius just behind the rotor plane and can be expressed as [25]:

$$r_1 = r_0\sqrt{\frac{1-a}{1-2a}} \tag{23}$$

where a represents the axial induction factor and its yawed form can be obtained as follows:

$$a = \frac{1-\sqrt{1-C_T\cos^2\gamma}}{2} \tag{24}$$

By applying mass conservation law in the deflected wake region and substituting Eq. (19) into Eq. (22), the final form of the proposed yaw wake model is derived and shown as Eq. (23):

$$\iint_{S_{elliptical}} U_w(x,y,z)dA = \iint_{S_{elliptical}} U(x,y,z)dA + \Delta m \tag{25}$$

$$U_w(x,y,z) = u_0(\frac{z}{z_0})^{\alpha} - u_0(1-\sqrt{1-\frac{C_T r_0^2\cos^2\gamma}{2\sigma(x)_y\sigma(x)_z}})e^{-(\frac{(y-\delta_y)^2}{2\sigma(x)_y^2}+\frac{(z-h_0)^2}{2\sigma(x)_z^2})} - \frac{2a\iint_{Sr_1}\Delta u dA}{\pi r_y r_z} \tag{26}$$

The proposed yaw wake model is able to better reflect the evolution of wake under yaw control because it takes into account not only the different rates of wake expansion due to the

vertical turbulence variation and ground effects but also the effect of the deflected rotor on wake expansion. More importantly, to the best of our knowledge, it is the first time that a yaw wake model is able to provide anisotropic wake expansion rates with generalization capability to account for wake deflection. By applying the proposed model, one can predict the deflected wake distribution in an accurate and computationally efficient manner without any posterior parameters.

3. Validation by the wind tunnel tests from WIRE Laboratory of EPFL

In order to ensure the accuracy and generalization capability of the developed yaw wake model, it is imperative to validate it using a comprehensive set of experimental data. Furthermore, two widely recognized yaw wake models have been chosen for comparative analysis. These models were selected due to their widespread acceptance in the field and their provision of general expressions for the wake expansion rate, as opposed to relying on parameters obtained post-hoc from specific cases. This comparative validation process will enable the assessment of the performance of the developed yaw wake model and ascertain its ability to accurately predict wake characteristics under yawed conditions.

The first is Jimenez [13] yaw wake model (Jimenez model hereafter) developed based on momentum conservation law and top-hat assumption. The second one is the Gaussian-based yaw wake model developed by Qian and Ishihara[16] (Qian model hereafter), which considers the ambient turbulence intensity, thrust coefficient, and yaw angle effects. For the detailed equations, please refer to *Appendix A* and *B*.

The availability of comprehensive wind tunnel data on yawed wake experiments conducted by Bastankhah and Porté-Agel [22], coupled with the utilization of a high-resolution stereoscopic particle image velocimetry (S-PIV) system, has been instrumental in this study. The wind tunnel experiments provided detailed flow field information spanning from 0D (D denotes the diameter of the model turbine) to 12D. This extensive dataset has facilitated the validation of both wake deflection and yawed wake distribution predicted by the developed yaw wake model. The use of the S-PIV system ensured accurate measurements and enabled a thorough examination of the wake characteristics, further enhancing the credibility and reliability of the validation process. The experiments were conducted in a closed-loop boundary-layer wind tunnel at the WIRE laboratory of EPFL, which has a test section of 2m height, 2.6m width, and 28m long. The inflow wind speed at hub height is 4.88 m/s with a power-law shear exponent of 0.178, and the corresponding turbulent intensity is

7.5%. The hub height of the miniature wind turbine is 0.125 m and the diameter of the rotor is 0.15m. The rotor is equipped with a DC generator to capture energy, while the tower base is mounted on the strain gauge sensor to measure the thrust force exposed on the wind turbine. According to the operated tip speed ratio (TSR), the corresponding thrust coefficient C_t under the unyawed condition is equal to 0.82.

Fig. 2 showcases the contours of the normalized streamwise wake distribution at hub height, as well as the trajectory of the deflected wake centreline from 0D to 12D. The figure depicts the results at yaw angles of 10°, 20°, and 30°, respectively. The white square line stands for the wake center trajectory of wind tunnel experimental data from Ref. [12]. To make a comparison, the simulation results are also given: the white line denotes the deflected wake centreline predicted by the proposed yaw wake model, while the white dash line and wind short dot line correspond to the simulated results of the Jimenez model and Qian model, respectively. As the yaw angle increases, it is observed that the wake loss at each flow position recovers more rapidly compared to milder yaw control. This phenomenon can be explained by the reduced energy extraction by the wind turbine from the incoming flow due to the yaw operation. The smaller momentum loss resulting from the reduced energy extraction is reflected in the faster recovery of the wake. Consequently, the wake loss diminishes more quickly as the yaw angle increases. Simultaneously, as the yaw angle increases, the lateral component of the thrust also increases. This increase in the lateral thrust component causes the wake centreline to deviate from its original trajectory, resulting in wake steering. According to the law of conservation of momentum, the lateral force induced by the increased lateral thrust component leads to the generation of a lateral wake velocity. This lateral wake velocity is responsible for the lateral displacement of the wake and contributes to the overall wake steering effect. As for the trajectory of the deflected wake centreline, the white line obtained by the proposed model follows the experimental data pretty well at both small and large yaw angles, especially from 0D to 7D, which is the main interest region where active yaw control may take place. The results indicate that the proposed wake deflection model tends to slightly overestimate the wake centreline in the downstream region of 8D to 12D. In comparison, the experimental data exhibits slight fluctuations in the downstream distance, which can be attributed to potential experimental errors. These fluctuations may arise from various factors such as measurement uncertainties, turbulence fluctuations, or other unaccounted variables. Despite these minor discrepancies, the overall agreement between the model predictions and experimental data suggests that the proposed wake deflection model

provides a reasonable estimation of the wake centreline under yawed conditions. The wake centreline predicted by Jimenez model deviates significantly from the experimental data and the gap increases with yaw angle and downstream distance, which is also indicated by many previous studies [12,16]. In most cases, the wake center trajectory predicted by Qian model is highly consistent with the proposed model. However, with the increase of yaw angle, the Qian model tends to slightly underestimate the results in the main wake region of concern for yaw control, namely from 0D to 5D, which is also illustrated in their paper [16]. In conclusion, both the proposed wake deflection model and the Qian model demonstrate acceptable accuracy in predicting the trajectory of the wake centerline. However, the proposed model exhibits better performance in predicting the region of primary interest for yaw control.

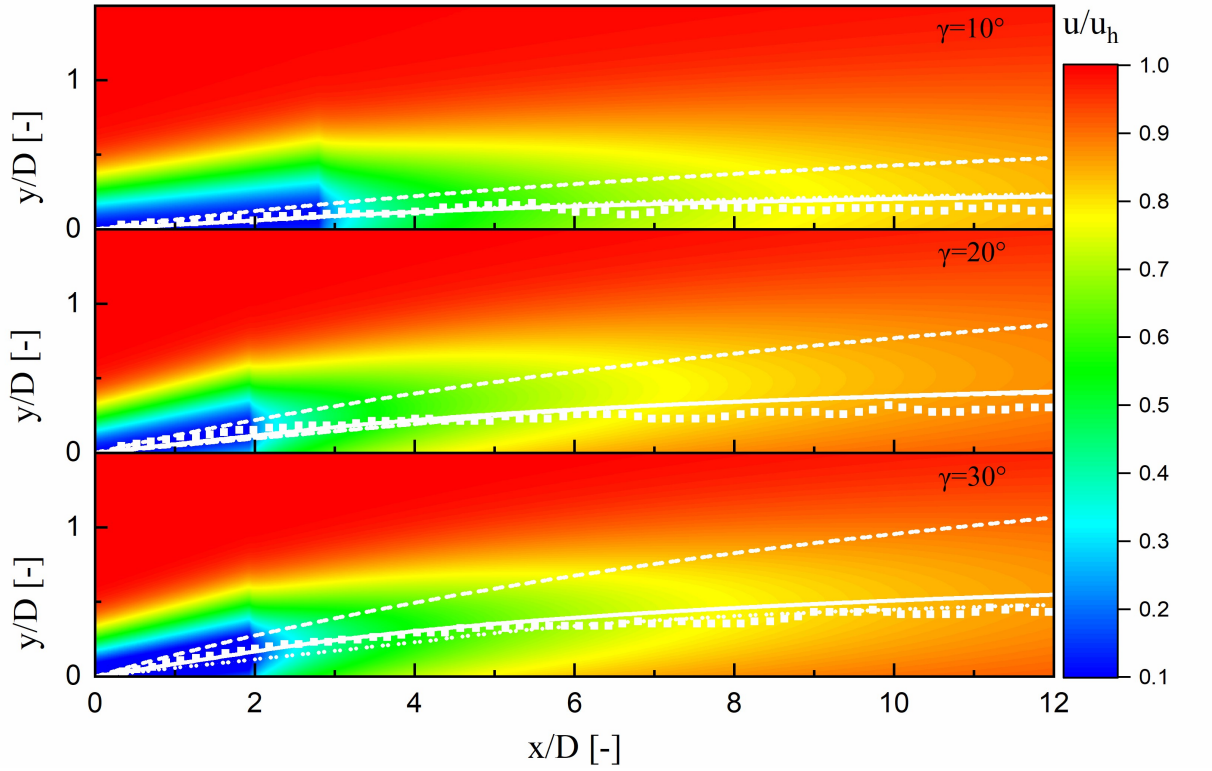

Fig. 2 Contours of the normalized streamwise wake velocity in the horizontal plane at hub height and the deflected wake center line due to yaw operations.

In order to conduct quantitative analysis on prediction accuracy, normalized root mean square error (NRMSE) [3] is adopted here to make a comparison. The equation is shown below:

$$NRMSE(y,\hat{y}) = \frac{\sqrt{\frac{1}{n}\sum_{i=1}^{n}(y_i - \hat{y}_i)^2}}{y_{\max} - y_{\min}} \tag{27}$$

where y_i is the measured value of the i-th sample for the model validation and $\hat{y}_i$ is the corresponding predicted value. $y_{\max}$ and $y_{\min}$ is the minimal and maximal value in the experimental dataset, respectively.

The NRMSE of the wake deflection prediction is compared among the proposed model and the counterparts in Table 1, in which the NRMSE of Qian model and Jimenez model is from Ref. [16]. It is found that all models predict more accurately as the yaw angle increases, although the results of Jimenez model show significant deviations compared with the other two models. The Qian model has the smallest NRMSE at all yaw angles, which proves its overall predictive ability on deflection forecasting. Upon comparing the results presented in this figure and Fig. 2, it can be noticed that the Qian model exhibits improved performance in the region 6D~12D than in the first half when subjected to larger yaw angles. On the contrary, the proposed model demonstrates higher accuracy in the region before 6D, which is of primary interest for the prediction of deflected wake behavior and active yaw control.

Table 1 NRMSE of the predicted wake deflection from the proposed yaw wake model and comparable models.

Yaw wake model	γ=10°	γ=20°	γ=30°
Jimenez [16]	1.38	1.16	0.94
Qian [16]	0.29	0.2	0.11
Proposed	0.32	0.26	0.14

Fig. 3 shows the deflected wake distribution with a yaw angle of 10° from 3D to 6D, which is the typical wind turbine interval range. Consequently, accurate prediction of wake distribution in this region is essential for conducting optimal active yaw control. As demonstrated in the figure, the proposed yaw wake model can predict the deflected wake distribution very well. It is found that the predicted results can perfectly fit the experimental data at a 4D distance while slightly underestimating the wake distribution around the wake center at the rest three locations. A slight deviation on the right side appears near 1D at all downstream locations as illustrated in the figure. Assuming that the horizontal wake distribution remains axisymmetric during yaw as well as being accurately predicted on the left side, the sudden jump in the measurements on the right side at around 1D could potentially be attributed to experimental error. In general, the proposed yaw wake model is able to

successfully forecast the wake width, wake deflection, and the maximal wake deficit under yaw conditions. Surprisingly, the Qian model remarkably underestimates the wake deficit around the wake center and overestimates it in the remaining region, although the trajectory of deflected wake center is well predicted. It can be seen that these deviations gradually decrease with the increase of downstream distance, but there remains a noticeable disparity between the simulation and experimental results. Regarding the results predicted by the Jimenez model, the figures below indicate that both the wake deflection and wake distribution are inaccurate with large deviations. To be specific, the wake center deflection is overestimated by the Jimenez model and the prediction inaccuracy increases with distance. On the other hand, the yawed wake distribution is largely underestimated with its top-hat assumption, while the prediction deviations decrease with streamwise locations. In addition, the wake width predicted by the Jimenez model underestimates the true value due to its linear wake width expression, making the wake distribution starts late at the left side while ending at approximately the same location as the experimental data.

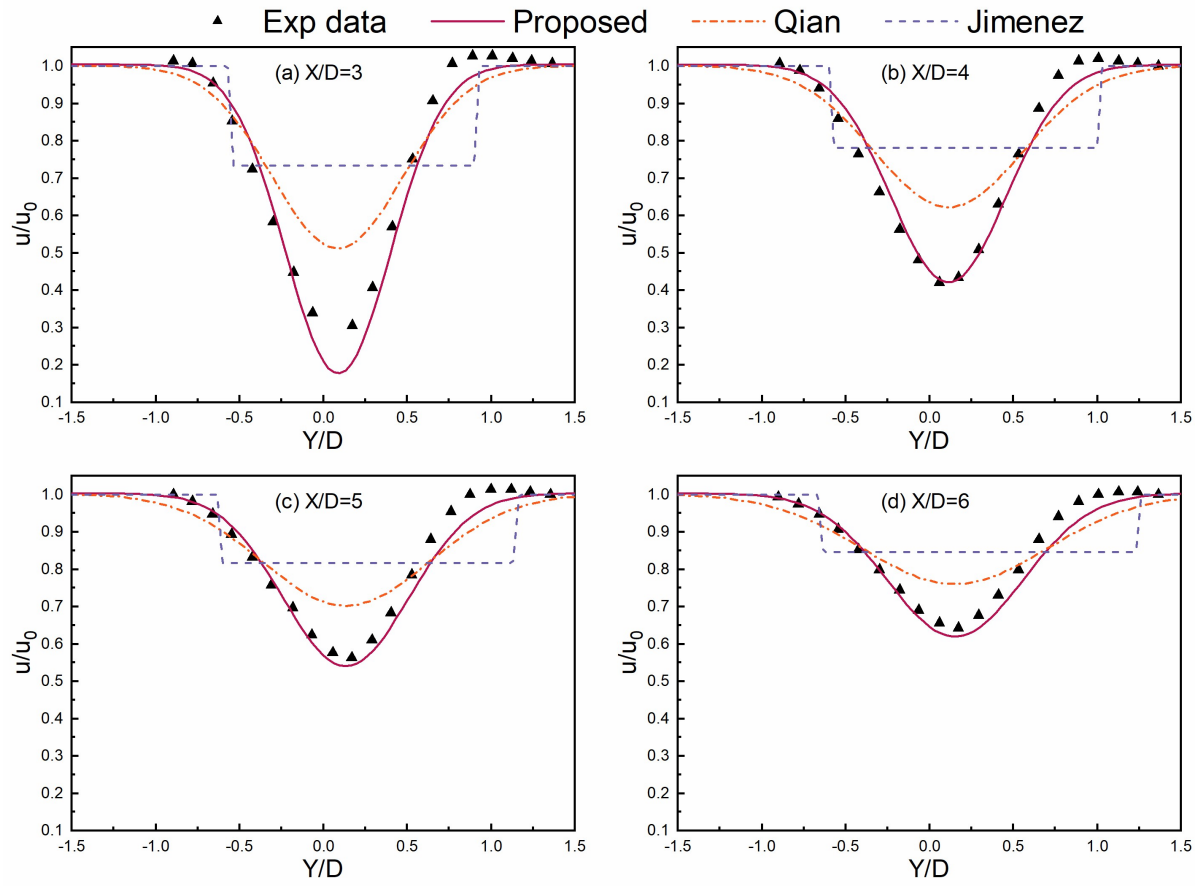

Fig. 3 Deflected wake distribution with a yaw angle of 10°.

Fig. 4 displays the predicted deflected wake distribution with a yaw angle of 20° from 3D to 6D, which is validated by experimental data as well as comparable models. It can be seen that the overall performance of the proposed model is still favorable at a relatively large yaw angle. The maximal wake deficit is accurately forecasted at 4D while marginally underestimating at 3D, 5D, and 6D. The predicted values of the maximum deficit at each downstream position are smaller than the corresponding values at a yaw angle of 10°. This can be attributed to the increased deflection of the rotor, which leads to a higher lateral component of the thrust force and a reduced flow component. Consequently, the velocity deficit in the wake is lower. The experimental results indicate that the yaw wake model accurately predicts the left side of the wake distribution. However, a similar sudden jump is observed on the right side of the wake at distances of 5D and 6D for the case with a yaw angle of 10°. This can be attributed to the factors mentioned earlier, such as experimental errors and potential limitations in accurately capturing the wake behavior in that specific region. As for comparison, the maximal wake deficit predicted by the Qian model is still significantly underestimated, and the predicted wake widths are larger than the measured ones. The relationship between prediction deviations and the yaw angle of this model is unclear. At 3D and 6D, the maximal wake deficits predicted by the Qian model tend to deviate the experimental data larger at the 20° yaw angle, while the situation is reversed at 4D and 6D. The Jimenez model predicts the minimal wake deficit and the largest wake deflection among the three yaw wake models. The wake center predicted by the Jimenez model at a large yaw angle tends to enlarge its difference from experimental data when compared with that under a small yaw angle. On the other hand, the predicted wake width is still smaller than the experimental data but may exceed it in the far wake region. Therefore, it is safe to conclude that the proposed model is capable of predicting the deflected wake center, yawed wake distribution, and wake width with favorable accuracy at both small and large yaw angles. Considering its good performance and general formula compared with other models, the proposed model is competent for accurate and highly efficient prediction of wake flow under yaw control, making contributions to the determinations of the optimal yaw control strategy.

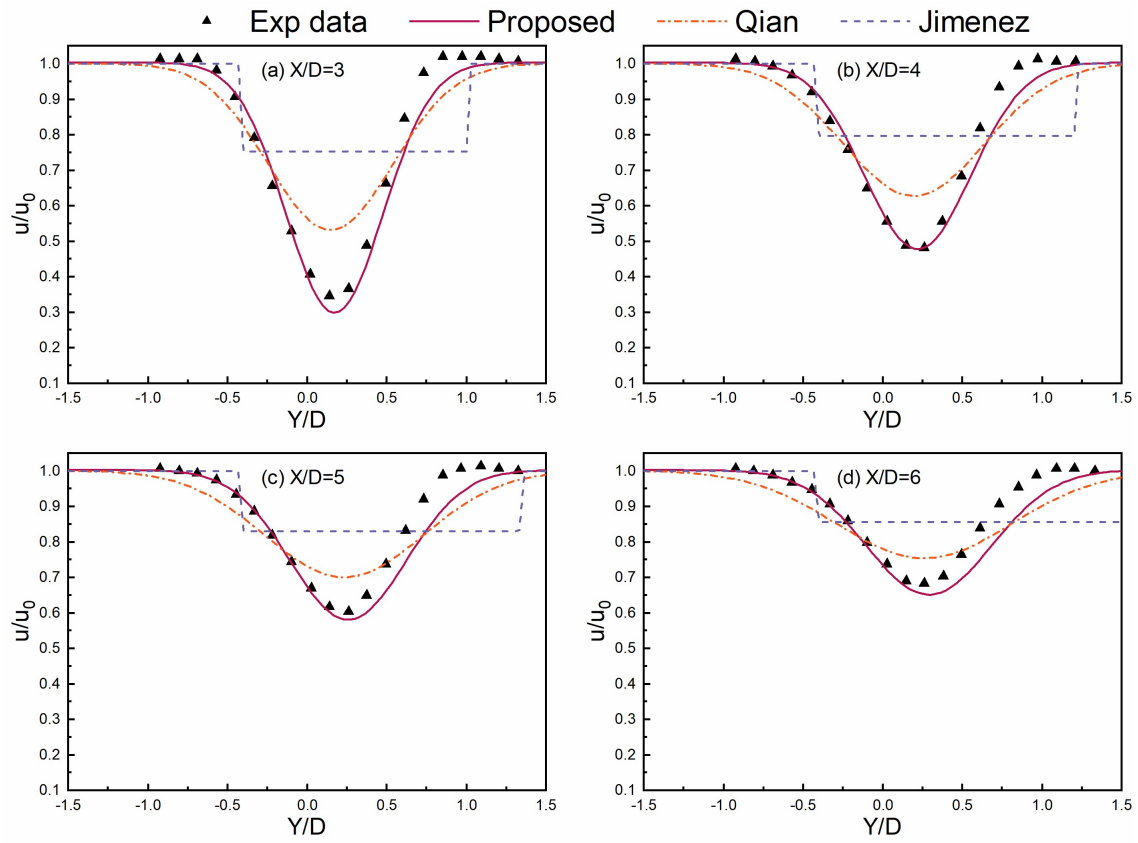

Fig. 4 Deflected wake distribution with a yaw angle of 20°.

For the purpose of error analysis, NRMSE of the predicted yaw wake distributions are illustrated in Fig. 5. It can be found that the best performance of the proposed model appears at 3D for both yaw angles. The overall deviation of this model is quite small, although the predictive deviations exceed 0.1 at 5D and 6D with a yaw angle of 20°, which is because of the inaccuracy that appeared on the right side as discussed before. The figure shows that the proposed model is capable of accurately predicting the wake distribution with acceptable deviation at various yaw operations and downstream locations, which validates its robustness. As a comparison, the NRMSE of Qian model is approximately two to three times larger than that of the proposed model, of which a larger yaw angle seems to have better performance at most locations in terms of predictive instability. The larger errors are attributed to the inaccuracy that appeared at maximal wake deficit prediction as well as the wake width prediction. Among the models compared, the Jimenez model exhibits the highest NRMSE at all tested conditions. The observed inaccuracy can be attributed to its reliance on the 1D top-hat assumption, as well as its tendency to overestimate wake deflection and wake width.

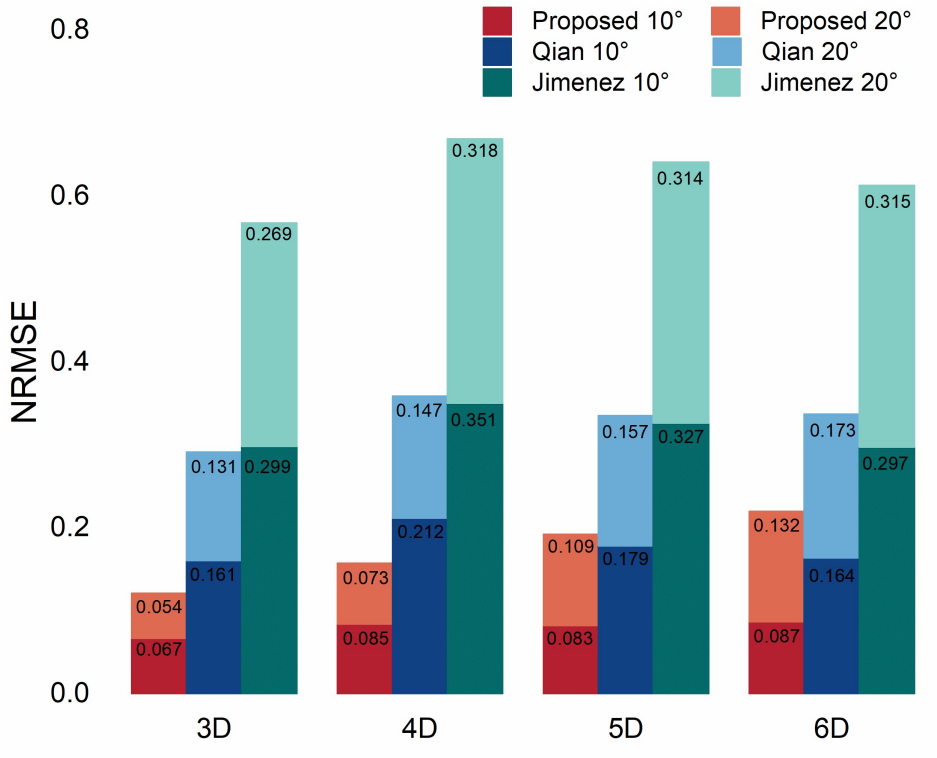

Fig. 5 NRMSE of the predicted wake distribution from the proposed yaw wake model and comparable models.

4. Wind tunnel experiments and model validation

4.1 Experimental setup and turbine model

In order to further validate the proposed yaw wake model, a series of wind tunnel experiments were conducted at the Department of Civil Engineering, The University of Hong Kong, using a low-speed closed-loop wind tunnel. The wind tunnel used in this study has a test section with dimensions of 3m width, 1.8m height, and 12m length. As illustrated in Fig. 6 (a), the wind tunnel setup included triangular spires and surface roughness elements, which were strategically designed to generate and control the turbulent atmospheric boundary layer (ABL) within the test section. The inflow condition adopted in this study is characterized by 8.4 m/s inflow wind speed at the hub height with a power-law shear exponent of 0.17 and a turbulent intensity of 14.4%. The wind turbine is installed at a place where it is fully immersed in the developed ABL.

The model wind turbine employed in this study has a hub height of 0.41 m and a rotor diameter of 0.45 m. The well-acknowledged airfoil geometry NREL S826 [26] is adopted to develop the blade shape. A JR3 force-torque torque sensor was employed to measure the

thrust force under various tip speed ratios by mounting it at the bottom of the miniature wind turbine. The blades and rotor hub are manufactured by 3D printing with AlSi10Mg Aluminum-magnesium alloy powder, which has the advantages of low density, high, strength and good corrosion resistance. On the other hand, the rest components including the nacelle, tower and tower base are made of steel.

Similar to the one developed in NTNU [27,28], active driving mode, which mainly consists of a servo motor and an encoder, is employed to drive the miniature wind turbine so that the rotational the speed of rotor can be directly adjusted stably with quick response. For the adopted wind turbine model, a 100W servo motor (Panasonic MSMF012L1U2M) is attached to the rear of the rotor with a maximum rotational speed of 3000rpm and da rives in counter-clockwise direction when observing from the upstream to downstream. A yawed wind turbine model with a positive direction is demonstrated in Fig. 6 (b).

The rotor-swept area of the model wind turbine is relatively small and its cross-section of the wind tunnel is within 10%. According to the conclusion drawn in Ref. [29], the blockage effect in this wind tunnel experiment can be neglected.

(a) Triangular spires and roughness elements.

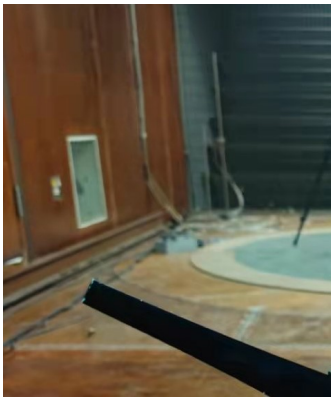

(b) Yawed wind turbine model.

Fig. 6 Experimental setup in the wind tunnel.

4.2 PIV measurements

In this study, a high-power particle image velocimetry (PIV) system from Dantec is employed to measure the wake flow field in the target field of view (FOV), which is a two-dimensional plane containing the two components (2D2C) of the wind speed. As illustrated in Fig. 7, the PIV system is mainly composed of a double cavity Q-switched neodymium-doped yttrium aluminum garnet (Nd:YAG) laser (Litron Nano L series) with an energy output of 50mJ at a wavelength of 532nm, a high volume liquid seeding generator (Dantec 10F03), a

high-speed CMOS camera (Dantec SpeedSense M120) with a resolution of 1920 pixel × 1200 pixel, and a synchronizer. Pure olive oil is responsible for generating seeding particles by using the seeding generator under approximately 3.3 bar, which ensures that the particles are light and small enough to follow the trajectory of the fluid. Then the aerosol particles within the measured plane are illuminated by a 2mm thick laser sheet generated from the laser beam passed through the cylindrical lens. The CMOS camera equipped with an AF Nikon 50mm lens is placed perpendicular to the illuminated plane with a suitable camera-objective distance. Finally, the synchronizer ensures the generation and collection of particle image pairs by synchronously powering the time sequence of the laser and high-speed CMOS camera.

For each trial in this study, 1800 image pairs are obtained by the above PIV system setting with a double frame mode. The time between pulses is set as 100μs to fix the initial and final positions of the captured particles. The image pairs are sampled with a frequency of 100Hz because the laser beam is optimized at this frequency, which provides the strongest luminance. The size of the Field of view is adjusted to 0.511× 0.319 m^2. First, the effect of electronic noise on the background is removed. After the image pair acquisition, the adaptive PIV algorithm [30] with high accurate sub-pixel interpolation scheme is adopted to generate the velocity vectors since it is capable of changing the size of the interrogation area (IA) based on the flow gradient and local seeding density. The size of the interrogation area (IA) is set as 32 pixel × 32 pixel and the overlap of interrogation area is 50%. According to Ref. [31], the uncertainty of PIV measurements in the velocity field, including systematic and statistics errors, is less than 3.5%.

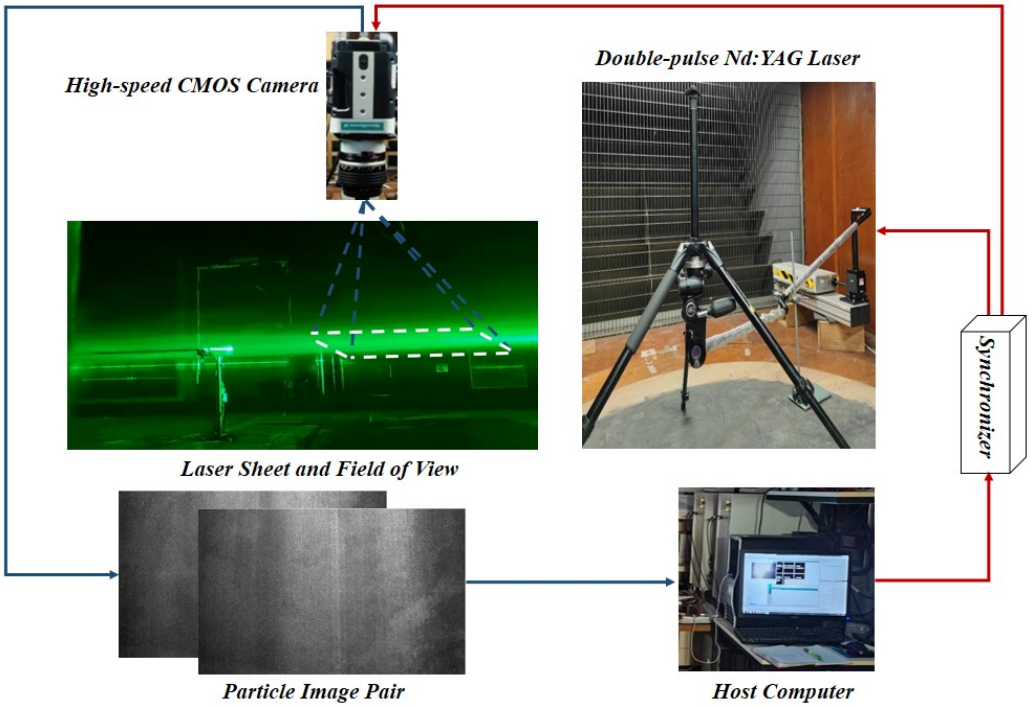

Fig. 7 PIV setup and measurements.

4.3 Results and validation

Fig. 8 present examples of streamwise velocity contours obtained through the PIV system at the hub height of the model wind turbine. The center of the field of view (FOV) is adjusted to align with the center of the nacelle of the model wind turbine., but there may exist displacement due to the masking of locations with limited or poor measurement. Nonetheless, these velocity contours provide valuable insights into the flow patterns and characteristics within the wake region, aiding in the validation and analysis of the yaw wake model. By adopting the 32 pixel × 32 pixel IA as mentioned above, a 60×38 vector map is used to represent the flow field at the measured place while setting the index skipping to make the vector map clear and intuitive.

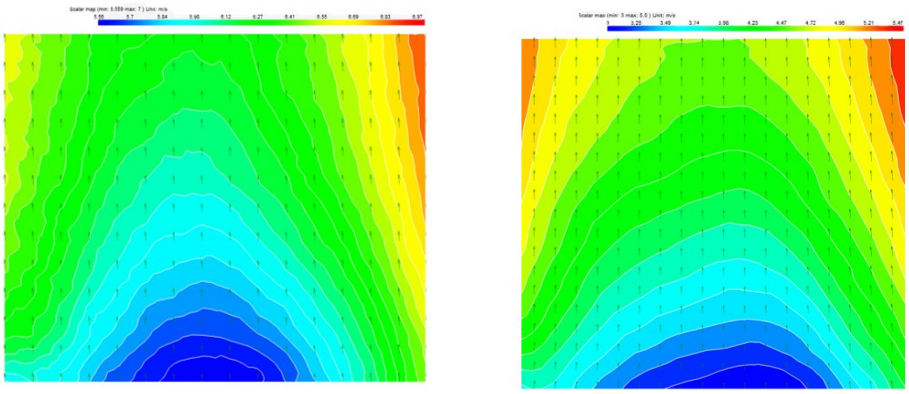

(a) Unyawed velocity contour. (b) Yawed velocity contour.

Fig. 8 Examples of horizontal velocity contours obtained from PIV measurements.

Fig. 9 displays the measured streamwise wind speed at hub height and the model validation with two comparable models. The center of the measured field of view is 2D from the model wind turbine and the measured thrust coefficient is 0.36. The abnormal measured data at margin regions could be attributed to various factors, such as insufficient laser intensity or the laser sheet not being perfectly horizontal. Insufficient laser intensity may result in weaker signal detection, leading to inaccurate velocity measurements. Similarly, if the laser sheet is not perfectly horizontal, it can cause distortions or uneven illumination across the measurement area, affecting the accuracy of the measured data. These factors should be considered when interpreting the results obtained from the PIV system in order to account for potential measurement limitations or uncertainties. The results show that the overall performance of the proposed model is favorable, although the predicted wake distribution tends to slightly overestimate the lateral wake recovery at some spanwise positions and the maximal wake deficit with gentle yaw operation. Apart from the prediction of wake center, Qian model can also fit the experimental data pretty well at unyawed conditions. However, this model seems to underestimate the maximal wake deficit at yaw conditions and the gap increases with yaw angle. As for the predicted wake width, it is close to the measured value at unyawed and small yaw angle but shows significant deviation at 20° yaw angle. The top-hat assumption of Jimenez model makes it fail to predict the wake distribution and the given wake expansion rate is admittedly too large.

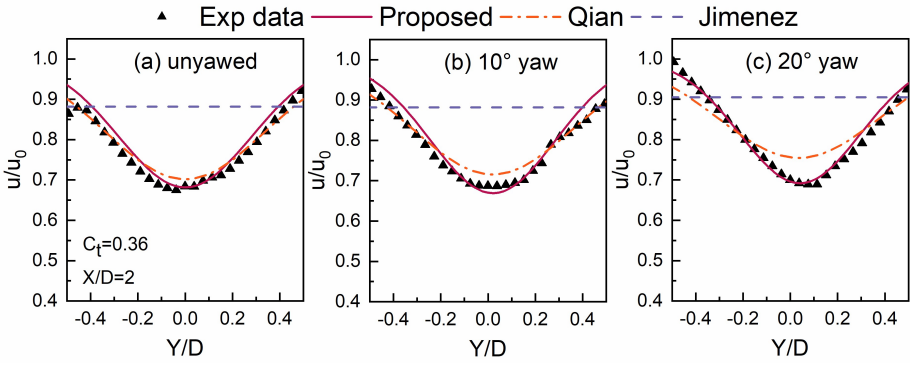

Fig. 9 Measurements and yaw wake model validation from wind tunnel tests at X/D=2.

Fig. 10 shows the wake distribution measurements at hub height and the corresponding comparisons at the downstream location X/D=3. To investigate the influence of thrust coefficient on yaw wake prediction, the thrust coefficient is decreased to 0.24 by adjusting the

rotational the speed of servo motor through the encoder. It seems that the abnormal measured data appears on both sides under unyawed condition and on the left side under yawed conditions, whose reasons have been discussed in the last paragraph. The predictions from proposed model exhibit overall consistency with the experimentally obtained wake distribution, where a small amount of irregular offset at 0.3D 10° yaw angle can be attributed to the non-ideal nature of the experimental environment. Similar to the case above, Qian model can predict the unyawed wake distribution relatively well. As for the yaw cases, it is found that the small thrust coefficient can improve the performance of Qian model in terms of the maximal wake deficit prediction, but the overestimation of wake expansion rate deteriorated. The relative error of Jimenez model is also decreased because of the small thrust coefficient. The comparisons demonstrate that the proposed model is capable of accurately predicting the yaw wake distribution at various yaw and operational conditions, which proves not only its accuracy but also its robustness.

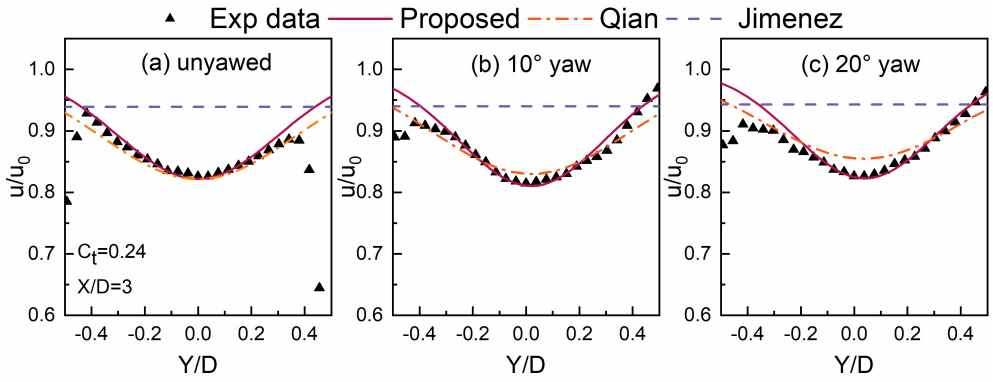

Fig. 10 Measurements and yaw wake model validation from wind tunnel tests at x/D=3.

Table 2 displays the NRMSE of the discussed yaw wake models against measured data. As NRMSE punishes the deviations remarkably, inaccurate measured data at marginal regions are neglected to truly reflect the predictive capacity of the yaw wake models. It can be demonstrated that the NRMSE of the Jimenez model is significantly larger than the other two models, although it decreases as yaw angle increases. As discussed before, Qian model can predict the unyawed wake distribution with favorable accuracy, however, the predictive error increases with the yaw angle. Compared with the above models, the proposed yaw wake model is able to perform pretty well at various yaw angles and operational conditions, which adequately reflects the accuracy and robustness of the proposed model.

Table 2 NRMSE of the predicted wake distribution from the proposed yaw wake model and comparable models.

Yaw wake model	2D γ=0°	2D γ=10°	2D γ=20°	3D γ=0°	3D γ=10°	3D γ=20°
Jimenez	0.56	0.49	0.43	0.81	0.54	0.59
Qian	0.08	0.1	0.13	0.1	0.11	0.14
Proposed	0.08	0.08	0.04	0.1	0.04	0.06

5. Summary and conclusions

This study presents a novel three-dimensional anisotropic yaw wake model aimed at accurately predicting the trajectory of wake deflection and wake distribution of the wind turbine under yaw operations. The proposed model is validated through two wind tunnel experiments, one sourced from a reputable previous study and the other conducted by the authors themselves. Through this comprehensive validation process, the superiority and generalization capability of the proposed yaw wake model are demonstrated. The main conclusions can be drawn as follows.

(1) The superiority of the proposed model is established through comparisons with other existing yaw wake models as well as two series of wind tunnel data. The results indicate that the proposed model exhibits satisfactory accuracy in predicting yaw wake characteristics, such as the wake width and maximal wake deficit. The variation of wake features is also described and explained physically. These findings confirm the efficacy of the proposed model in accurately capturing the essential features of yawed wakes.

(2) Meanwhile, the generalization capability of the proposed model has been demonstrated. Through two sets of experimental validations, it has been shown that the proposed model is able to accurately estimate the yawed wake of wind turbines with both high thrust coefficient (usually for utility-scale WTs) and small one (usually for miniature WTs). Additionally, the model accurately predicts the wake characteristics at different downstream locations within the primary interest region. This indicates that the proposed model is capable of accurately estimating the yawed wake for various wind turbine configurations and operating conditions, making it a versatile and reliable tool.

(3) The wake expansion rates proposed in this study are designed to capture the elliptical wake cross-section resulting from yaw operation. This consideration ensures that the proposed yaw wake model accurately represents the physical characteristics of the wake. More importantly, the given wake expansion rates are the functions of easily available parameters

such as inflow velocity, turbulence, and the thrust coefficient, which guarantees the generalization capability of the proposed expressions of the wake expansion rate.

(4) As for the wake deflection model, the accuracy of which is validated against the trajectory of the wake centreline measured in the wind tunnel experiment. The results show that the developed model closely aligns with the measured data, especially at relatively large yaw angles and in the region before 7D, which is of primary interest for active yaw control. This validation confirms the effectiveness and reliability of the proposed wake deflection model, highlighting its potential for practical applications in optimizing wind turbine performance through yaw control strategies.

The proposed analytical yaw wake model is the first attempt to provide anisotropic and general wake expansion rates to consider the deflected wake distribution caused by yaw operation. Consequently, it can predict the wake deflection and yawed wake distribution in an accurate and cost-efficient manner, which is crucial for further applications of this model such as active yaw control.

Declaration of Competing Interest

The authors declare that they have no known competing financial interests or personal relationships that could have appeared to influence the work reported in this paper.

Acknowledgment

The work described in this paper was supported by the Research Institute for Sustainable Urban Development (RISUD), The Hong Kong Polytechnic University. The authors would also like to express their gratitude to Prof. K M Lam from the University of Hong Kong, Mr. Haoyun Shi from the City University of Hong Kong and Mr. Yao Zhang from Dantec for their support to complete the wind tunnel tests.

Appendices

Appendix A. Jimenez wake deflection model

Jimenez et al. [13] developed the first yaw wake model based on 1D Jensen model [14] and therefore gave a top-hat shape yawed wake prediction. The wake deflection is considered to be induced by the lateral component of thrust force. A concept of control volume was adopted to conduct momentum conservation between the far upstream and yawed wake. The expression of skew angle and wake deflection model can be written as:

$$\theta(x) = \frac{C_T \cos^2\gamma \sin\gamma}{2\left(1 + 2k_w x / D\right)} \tag{A.1}$$

$$\frac{\delta_y(x)}{D} = \cos^2\gamma \sin\gamma \frac{C_T}{4k_w}\left(1 - \frac{1}{1 + 2k_w x / D}\right) \tag{A.1}$$

where k_w is the wake expansion rate and equals to $0.4I_0$.

Appendix B. Qian yaw wake model

Based on a framework similar to the Jimenez's model [13], Qian and Ishihara [16] proposed a more advanced 3D yaw wake model while also applying momentum conservation over a control volume. The yaw wake model can be written as:

$$U_w = U_0\left(F(C_T^{'}, I_0, x/D)\exp\left(-\frac{r'^2}{2\sigma^2}\right)\right) \tag{B.1}$$

where the spanwise distance from the wake center $r' = \sqrt{x^2 + (y + \delta_y)^2}$ and

$$F(C_T^{'}, I_0, x/D) = \frac{1}{\left(a + b \cdot x/D + p\right)^2} \tag{B.2}$$

where the thrust coefficient under yaw control $C_T^{'} = C_T \cos^3\gamma$ and

$$a = 0.93C_T^{'-0.75}I_0^{0.17},\ b = 0.42C_T^{'0.6}I_0^{0.2},\ p = \frac{0.15C_T^{'-0.25}I_0^{-0.7}}{(1 + x/D)^2} \tag{B.3}$$

The skew angle in far wake can be expressed as:

$$\theta(x) = \frac{C_T \cos^2\gamma \sin\gamma}{44.4\left(\sigma(x)/D\right)^2 - 1.88C_T \cos^3\gamma} \tag{B.4}$$

Therefore, the deflection in far wake region can be derived by integrating from initial downstream position x0 to far wake and given as:

$$\frac{\delta_y(x)}{D} = \frac{\sqrt{C_T \cos\gamma}\sin\gamma}{18.24k^*} \ln\left|\frac{\left(\sigma_0/D + 0.24\sqrt{C_T\cos^3\gamma}\right)\left(\sigma(x)/D - 0.24\sqrt{C_T\cos^3\gamma}\right)}{\left(\sigma_0/D - 0.24\sqrt{C_T\cos^3\gamma}\right)\left(\sigma(x)/D + 0.24\sqrt{C_T\cos^3\gamma}\right)}\right| + \frac{\delta_y(x_0)}{D} \tag{B.5}$$

Then, the linearly developed deflection in near wake region can be expressed as:

$$\frac{\delta_y(x)}{D} = \theta_0 \frac{x}{D} \tag{B.6}$$

The length of near wake and initial standard deviation were obtained mathematically by equating the formula of the initial skew angle given by Coleman [23] and the skew angle in the far wake. Note that the formula of x_0 is not intended to accurately predict the near wake length, but to provide an initial value for the yaw wake prediction in the far wake.

$$\frac{\sigma_0}{d} = \sqrt{\frac{C_T \cos^2\gamma(\sin\gamma + 1.88\cos\gamma\theta_0)}{44.4\theta_0}} \tag{B.7}$$

$$\frac{x_0}{d} = \left(\frac{\sigma_0}{d} - \varepsilon\right) \Big/ k \tag{B.8}$$

References

[1] Lee J, Zhao F. GWEC Global Wind Report. Glob Wind Energy Counc 2022:75.

[2] Nash R, Nouri R, Vasel-Be-Hagh A. Wind turbine wake control strategies: A review and concept proposal. Energy Convers Manag 2021;245:114581. https://doi.org/10.1016/j.enconman.2021.114581.

[3] He R, Yang H, Sun S, Lu L, Sun H, Gao X. A machine learning-based fatigue loads and power prediction method for wind turbines under yaw control. Appl Energy 2022;326:120013.

[4] Yang S, Deng X, Ti Z, Yan B, Yang Q. Cooperative yaw control of wind farm using a double-layer machine learning framework. Renew Energy 2022;193:519–37. https://doi.org/10.1016/j.renene.2022.04.104.

[5] Kumar D, Rotea MA, Aju EJ, Jin Y. Wind plant power maximization via extremum seeking yaw control: A wind tunnel experiment. Wind Energy 2022:283–309. https://doi.org/10.1002/we.2799.

[6] Dou B, Qu T, Lei L, Zeng P. Optimization of wind turbine yaw angles in a wind farm using a three-dimensional yawed wake model. Energy 2020;209:118415. https://doi.org/10.1016/j.energy.2020.118415.

[7] Urbán AM, Larsen TJ, Larsen GC, Held DP, Dellwik E, Verelst D. Optimal yaw

strategy for optimized power and load in various wake situations. J Phys Conf Ser 2018;1102. https://doi.org/10.1088/1742-6596/1102/1/012019.

[8] Fleming P, King J, Simley E, Roadman J, Scholbrock A, Murphy P, et al. Initial results from a field campaign of wake steering applied at a commercial wind farm – Part 1. Wind Energy Sci 2020;5:945–58. https://doi.org/10.5194/wes-5-945-2020.

[9] Zong H, Porté-Agel F. A point vortex transportation model for yawed wind turbine wakes. J Fluid Mech 2020;890:1–25. https://doi.org/10.1017/jfm.2020.123.

[10] Medici D, Alfredsson PH. Measurements on a wind turbine wake: 3D effects and bluff body vortex shedding. Wind Energy An Int J Prog Appl Wind Power Convers Technol 2006;9:219–36.

[11] Howland MF, Bossuyt J, Martínez-Tossas LA, Meyers J, Meneveau C. Wake structure in actuator disk models of wind turbines in yaw under uniform inflow conditions. J Renew Sustain Energy 2016;8:12–6. https://doi.org/10.1063/1.4955091.

[12] Bastankhah M, Porté-Agel F. Experimental and theoretical study of wind turbine wakes in yawed conditions. J Fluid Mech 2016;806:506–41. https://doi.org/10.1017/jfm.2016.595.

[13] Ángel Jiménez AC and EM. Application of a LES technique to characterize the wake defl ection of a wind turbine in yaw. Wind Energy 2013:1–20. https://doi.org/10.1002/we.

[14] Jensen NO. A note on wind generator interaction 1983.

[15] Shapiro CR, Gayme DF, Meneveau C. Modelling yawed wind turbine wakes: A lifting line approach. J Fluid Mech 2018;841:R11–112. https://doi.org/10.1017/jfm.2018.75.

[16] Qian GW, Ishihara T. A new analytical wake model for yawed wind turbines. Energies 2018;11. https://doi.org/10.3390/en11030665.

[17] He R, Yang H, Sun H, Gao X. A novel three-dimensional wake model based on anisotropic Gaussian distribution for wind turbine wakes. Appl Energy 2021;296:117059.

[18] Shengbai Xie. Self-similarity and turbulence characteristics of wind turbine wakes via large-eddy simulation. Wind Energy 2013:1–20. https://doi.org/10.1002/we.

[19] Abkar M, Porté-Agel F. Influence of atmospheric stability on wind-turbine wakes: A large-eddy simulation study. Phys Fluids 2015;27. https://doi.org/10.1063/1.4913695.

[20] Tennekes H, Lumley JL. A First Course in Turbulence. 1972. https://doi.org/10.7551/mitpress/3014.001.0001.

[21] Burton T, Sharpe D, Jenkins N, Bossanyi E. Wind energy handbook. vol. 2. Wiley Online Library; 2001.

[22] Bastankhah M, Porté-Agel F. Experimental and theoretical study of wind turbine wakes in yawed conditions. J Fluid Mech 2016;806:506–41. https://doi.org/10.1017/jfm.2016.595.

[23] Coleman RP, Feingold AM, Stempin CW. Evaluation of the induced-velocity field of an idealized helicoptor rotor. National Aeronautics and Space Administration Hampton Va Langley Research Center; 1945.

[24] Gao X, Li B, Wang T, Sun H, Yang H, Li Y, et al. Investigation and validation of 3D wake model for horizontal-axis wind turbines based on filed measurements. Appl Energy 2020;260. https://doi.org/10.1016/j.apenergy.2019.114272.

[25] Gao X, Yang H, Lu L. Optimization of wind turbine layout position in a wind farm using a newly-developed two-dimensional wake model. Appl Energy 2016;174:192–200. https://doi.org/10.1016/j.apenergy.2016.04.098.

[26] Bartl J, Mühle F, Schottler J, Sætran L, Peinke J, Adaramola M, et al. Wind tunnel experiments on wind turbine wakes in yaw: Effects of inflow turbulence and shear. Wind Energy Sci 2018;3:329–43. https://doi.org/10.5194/wes-3-329-2018.

[27] P. -Å. Krogstad1 and J. A. Lund. An experimental and numerical study of the performance of a model turbine. Wind Energy 2012:1–20. https://doi.org/10.1002/we.

[28] Schümann H, Pierella F, Sætran L. Experimental investigation of wind turbine wakes in the wind tunnel. Energy Procedia 2013;35:285–96. https://doi.org/10.1016/j.egypro.2013.07.181.

[29] Krogstad P åge, Eriksen PE. "Blind test" calculations of the performance and wake development for a model wind turbine. Renew Energy 2013;50:325–33. https://doi.org/10.1016/j.renene.2012.06.044.

[30] Wieneke[1] B, Pfeiffer[1] K. Adaptive PIV with variable interrogation window size and shape 2010.

[31] Cao X, Liu J, Jiang N, Chen Q. Particle image velocimetry measurement of indoor airflow field: A review of the technologies and applications. Energy Build 2014;69:367–80.